Microstructure of high modulus solid state extruded polyethylene: 1. Electron microscopy studies of 12, 24 and 36 × *EDR*

Edward S. Sherman, Roger S. Porter and Edwin L. Thomas*
Polymer Science and Engineering Department, Materials Research Laboratory, The University of Massachusetts, Amherst, Massachusetts 01003, *USA*
(*Received* 28 *November* 1979; *revised* 14 *September* 1981)

The microstructure of a series of solid state extruded polyethylenes for two molecular weights (M_w=59 000 and 200 000) were examined by electron microscopy. The sample extrusion draw ratio varied from 12–24–36 ×. The axial tensile modulus increases almost linearly with draw ratio from 10 GPa (12 ×) to 40 GPa (36 ×). The extrudates consist of ribbon-like aggregates of 120–250 Å diameter microfibrils. Dark field electron microscopy indicates an increase of the average axial crystallite size with increasing extrusion draw ratio. The 12 and 24 × lower molecular weight samples have microstructures similar to conventionally drawn fibres, i.e. crystalline regions alternate with noncrystalline regions along the fibre axis. The low molecular weight 36 × sample and the high molecular weight 24 × sample contain broader crystalline size distributions and a small component of very long crystals (1000–8000 Å). Moreover, individual fibrils of these highest modulus extrudates do not display fibre symmetry but consist rather of sequences of diffracting crystallites (crystallite colonies) indicating, by their coherence, the presence of thin intercrystalline bridges or needle crystals.

Keywords Structure; microscopy; electron; extrusion; solid state; polyethylene; fibres; microstructure; dark field

INTRODUCTION

A continuing goal of research in high modulus fibres from flexible chain molecules is to further optimize processing conditions to produce high tensile modulus and strength both quickly and inexpensively. The ideal morphology would consist of fully extended and uniaxially aligned molecules. Such an achievement will require a detailed knowledge of the effect of deformation on morphology and how morphology relates to resultant physical properties.

The realization that polymers could be deformed to form strong fibres dates from the early part of this century; the first commercial use being the introduction of Nylon-6,6 by the du Pont Company. Since then, a great deal of theoretical and experimental work has been conducted towards understanding fibre structure and properties. Reasonable models are available for the deformation process, fibre structure and properties for cold drawn polymers such as polyethylene (PE)[1] and nylon[2]. Since the production of high modulus PE by solid state extrusion[3], hot drawing[4] and stirred solution spinning[5]; new structural models have been proposed to account for the unusual properties of these materials. The tensile modulus of such fibres can be a significant fraction of the theoretically calculated modulus of PE (~324 GPa[6]) depending on conditions[7].

The results of Capaccio and Ward, Barham and Keller[9] and Wu *et al.*[10] show that the modulus of hot drawn PE is a linear function of draw ratio over the range 6–30X. A fibre with draw ratio of 25–30X can yield a tensile modulus of approximately 60 GPa, for a variety of combinations of polymer molecular weight, drawing temperature and deformation rate. Similar results have been obtained for solid state extruded PE where the tensile modulus has been shown to increase linearly with extrusion draw ratio (*EDR*) from 12–40X[11,12]. Other properties which are indirect measures of the microstructure, such as birefringence, melting point, thermal expansion coefficient and *c*-axis orientation function, however, reach plateau values in the range of 40X[12].

Our approach is to combine electron microscopic, wide and small angle X-ray scattering techniques, to gain a better understanding of the actual microstructures present in ultra high modulus PE produced by solid state extrusion. The influence of extrusion draw ratio on sample morphology is investigated for a series of samples of 12, 24 and 36X *EDR* and for the 24X sample, the effect of molecular weight is examined. In this paper (1) we report the mechanical properties and principally on the electron microscopic results. Wide and small angle X-ray scattering results and a general discussion of the appropriate microstructural model for solid state extruded PE are presented in an accompanying paper (2)[13].

Review of structural models

Many models for describing the morphology of high modulus fibres have been proposed. These models represent the latest versions of the continuing evolution of

* To whom correspondence should be sent

0032-3861/82/071069-08$03.00

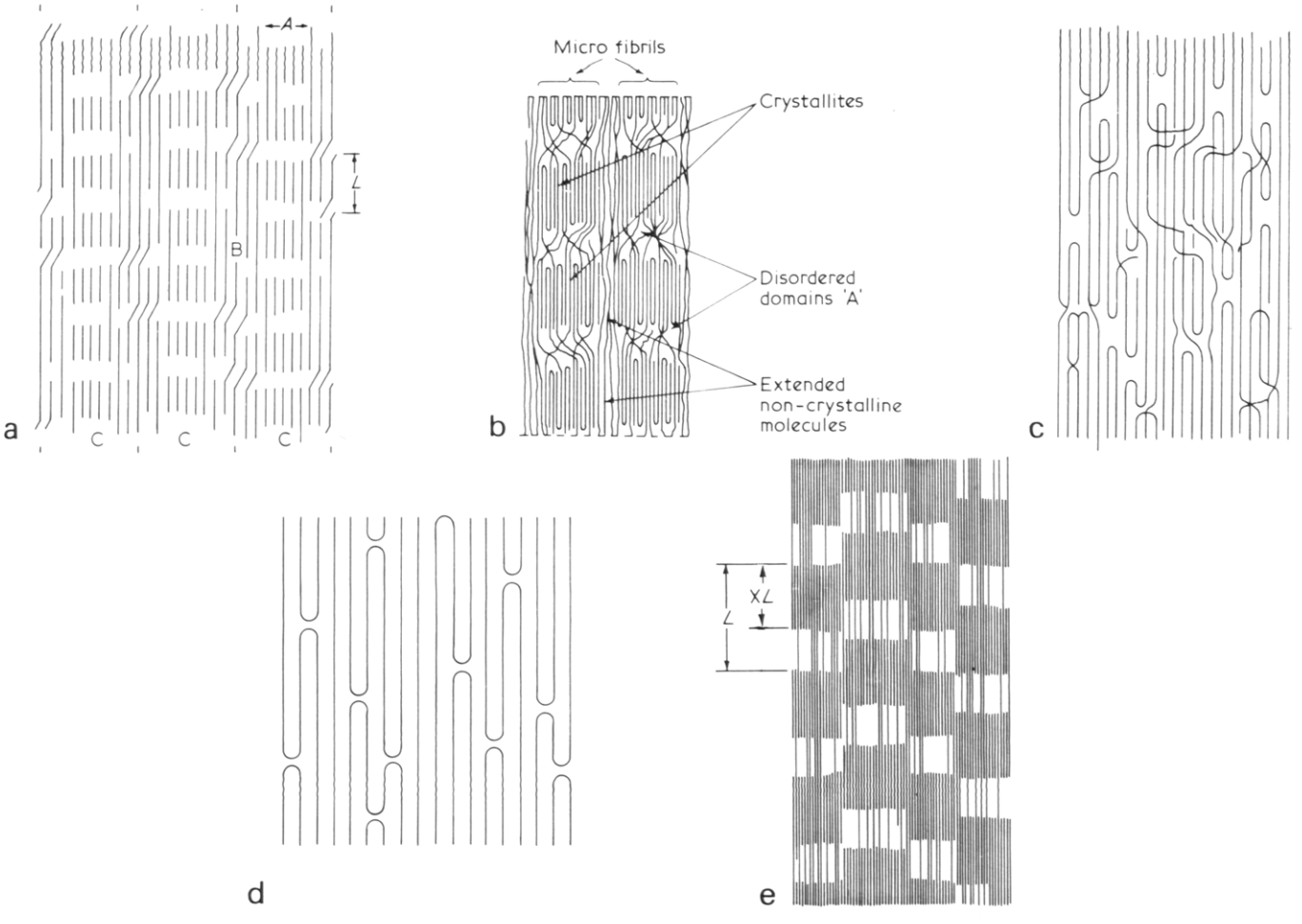

Figure 1 (a) Peterlin's model for cold drawn microfibres (Reference 18). (b) Prevorsek's model for Nylon-6 (Reference 19). (c) Fischer's model for drawn fibres (Reference 20). (d) Clark's model for drawn fibres (Reference 22). (e) Ward's model for hot drawn and solid state extruded fibres (References 23 and 24)

the molecular structure of fibres based on the early ideas of Mark[14], Staudinger[15] and (later) those of Hess and Kiessig[16]. Microfibrils have been identified by Peterlin[17] as the key microstructural element responsible for fibre properties. Microfibrils may be typically ~200 Å wide and 15–20 μm long and consist of alternating crystal blocks and noncrystalline regions connected by taut tie molecules[18]. *Figure 1a* shows Peterlin's model with intrafibrillar tie molecules (TM) at A, interfibrillar TM (B) and the microfibrils (C). The axial modulus is a function of the number of load bearing tie molecules that cross the noncrystalline regions to connect adjacent crystalline blocks along the microfibre.

Prevorsek *et al.*[19] have proposed a structural model (specifically for Nylon-6 fibres) that is shown in *Figure 1b*. They consider the microfibrils to be the soft phase with extended but non-crystalline molecules between the microfibrils as the stiff phase. *Figure 1c* is the model proposed by Fischer and Goddar[20] for unannealed highly drawn fibres. The microstructure consists of a homogeneous crystalline matrix with a high concentration of defects (primarily chain folds and chains crossing normal to the fibre axis) not completely statistically distributed so as to give rise to a periodic density fluctuation along the fibre axis. The continuous crystal models of Porter[21] and Clark[22] for ultradrawn fibres also feature a homogeneous, primarily extended chain crystalline matrix containing defects without any axial periodicy (see *Figure 1d*). Ward *et al.*[23,24] have recentiy extended Peterlin's model to include 'crystalline bridges', formed from groups of crystallized taut tie molecules between the crystallites (see *Figure 1e*). The cross sectional area of the crystalline bridges is assumed to be considerably less than that of the individual microfibril.

These structural models, while all emphasizing highly oriented chains, disagree as to whether the high modulus fibre consists of a discrete lateral microfibril structure with crystallites axially connected in various ways or a homogeneous continuous crystalline matrix with various defects. The calculated fibre modulus for these model structures is assumed to be a function of the theoretical crystal modulus and the amorphous modulus, combined via the volume fractions and distributions of the microstructural elements.

There are several direct techniques that have been used to determine the existence and/or quantity of these various structural elements. Clark has suggested that the lack of a small angle X-ray maximum for his 'superdrawn' acetal fibres supports a continuous crystal structure[22]. Ward's group has used wide angle X-ray diffraction (WAXD) line breadth analysis (of the (002) reflection) in conjunction with small angle measurement of the long period in PE drawn at 75°C[23,24]. The crystal sizes measured by WAXD and SAXS were used to calculate the fraction of intercrystalline bridges. They have also recently measured the crystallite size distribution of hot

(120°C) drawn PE by dark field (DF) microscopy of microtomed longitudinal sections[25]. Grubb and Keller[26] also used DF to determine the crystallite size distribution which they found to be of the most probable type in stirred solution grown PE fibrils. They suggested the axial crystalline regions were limited in extent due to defects such as trapped entanglements and dislocations. Chanzy *et al.*[17] used DF imaging to show the extended chain nature of cellulose fibrils and Petermann *et al.*[28] have imaged micron long needle crystals in PE and isotactic polystyrene.

Several indirect methods such as gel permeation chromatography[29], thermal expansion[30] and differential scanning calorimetry[31] have also been applied to solid state extruded PE.

Samples

Details of the solid state extrusion technique have been described previously[3]. Here, two high density polyethylenes are used. These are Alathon® 7050, having $M_w = 59\,000$ and $M_w/M_n = 3$ (designated samples A-1, A-12, A-24, A-36) and Marlex® 6003 having $M_w = 200\,000$ and $M_w/M_n = 7$–13 (sample M-24). These polymers were solid state extruded using an Instron capillary rheometer starting from bulk spherulitic billets that had been moulded by melting and slow cooling. The billets were extruded at 120°C and 2400 atmospheres through a conical die of 20° semiangle. The draw ratio is set by the die geometry and was varied from 12–24–36X. The A samples were extruded as whole billets, whereas sample M-24 was extruded as a billet split in half. The details of the split billet technique have also been previously described[32]. The split billet technique was used for the higher molecular weight sample for two reasons: (1) a split billet extrudes at a much faster rate than the corresponding whole billet under the same extrusion conditions and (2) when extruded as a split billet, the M-24 sample has a higher tensile modulus than the whole billet extrudate. This is because the split in the extrudate relieves the radial stress component associated with the tendency for the extrudate to expand (i.e., die swell)[33]. The lower molecular weight samples A yield extrudates of identical tensile moduli whether extruded as a whole or split billet. This is reasonable since the magnitude of the normal force is molecular weight dependent. Samples of A for both split and whole billets show identical flow profiles. The extrusion rates for A-12, A-24 and A-36 samples were 45, 20 and 1.4 mm min^{-1} and for the M-24 sample, 0.6 mm min^{-1}. The A-24 and M-24 samples are the same in preparation except for the difference in molecular weight and rate of extrusion.

EXPERIMENTAL

Electron microscopy

Thin specimens for transmission electron microscopy (*TEM*) were obtained by two independent methods. Detachment replicas were obtained by initial longitudinal freeze fracturing of the sample at liquid nitrogen temperature to expose the interior morphology. This internal fracture surface was then carbon-platinum shadowed at 30° followed by carbon at 90°. A polyacrylic acid (PAA) solution was then painted on the surface, allowed to dry and then stripped off, detaching the C-Pt/C replica and most importantly, thin polymer fibrils which adhere well to the replica. The replica was then cut into small pieces and thoroughly washed in distilled water to remove all the PAA and then mounted on grids for microscopy.

The second method involved etching the extruded sample in red nitric acid[34,35] for two weeks at 70°C. The samples were then washed with water, and low molecular weight fragments were removed by extraction with hot acetone vapours. Fibrous etch fragments were dispersed by mild ultrasonication in ethanol. The suspension of fragments was then simply allowed to dry on a carbon support film mounted on a *TEM* grid.

Bright field (BF) and dark field (DF) electron microscopy were performed using a JEOL 100CX 'TEMSCAN' in both the conventional transmission electron microscope (*CTEM*) mode and as a scanning transmission electron microscope (*STEM*)[36]. *CTEM*-DF was performed on the detachment replicas using the combined 110 and 200 reflections. Annular *n*-beam *STEM*-DF was performed on the etch fragments and the detachment replicas using all the reflections out ot and including the 002. Comparison of the DF images from the detachment replicas and etch fragments permitted the assessment of specimen preparation techniques on the observed morphology.

Electron beam radiation damage limits the obtainable information due to loss of crystallinity and dimensional changes[37]. The microscope is therefore operated with low electron flux on the sample and with minimal damage accomplished by focusing on adjacent areas, rapidly translating to a new area and then recording the DF image using approximately 60% of the measured radiation lifetime[38]. Both Kodak Electron Image Film 4463 and du Pont Cronex 'low-dose' X-ray film were used.

Nitric acid digestion was also used to prepare longitudinal sections of the extruded fibres for examination by secondary electron imaging (*SEI*). A short piece of each extrudate was immersed in 100% HNO_3 for 8, 16 and 24 h for the 12, 24 and 36 EDR samples, respectively[39]. After washing and drying, the now very brittle fibre was placed in liquid nitrogen and fractured along the axial direction. Samples were then sputter coated with approximately 300 Å of gold and examined in an ETEC U-1 SEM at 20 kV.

D.s.c. scans were performed at a heating rate of 10°C min^{-1}, using a Perkin-Elmer DSC-2. An induim sample was used to calibrate melting point and heat of fusion. The degree of crystallinity was calculated assuming 68 cal/gram for the heat of fusion of PE crystals[40].

Sample densities were measured in an ethylene glycol–isopropanol gradient column by ASTM procedure D1505-68 using glass calibration beads. The clarity of the extrudates along with other information indicate a negligible void content. Density measurements were reproducible to 0.0005 gm cm^{-3}.

The modulus measurements of the extrudates were performed in tension at ambient temperature on an Instron TTM tensile tester. The elastic modulus was determined from the tangent to the stress–strain curve at 0.1% strain. The strain was measured using an extensometer. The strain rate was 3×10^{-5} s^{-1} and initial sample diameters were 1–3 mm for the 12, 24 and 36 EDR, respectively. No corrections were made for limited gauge length, which generally leads to moduli up to 20% too low.

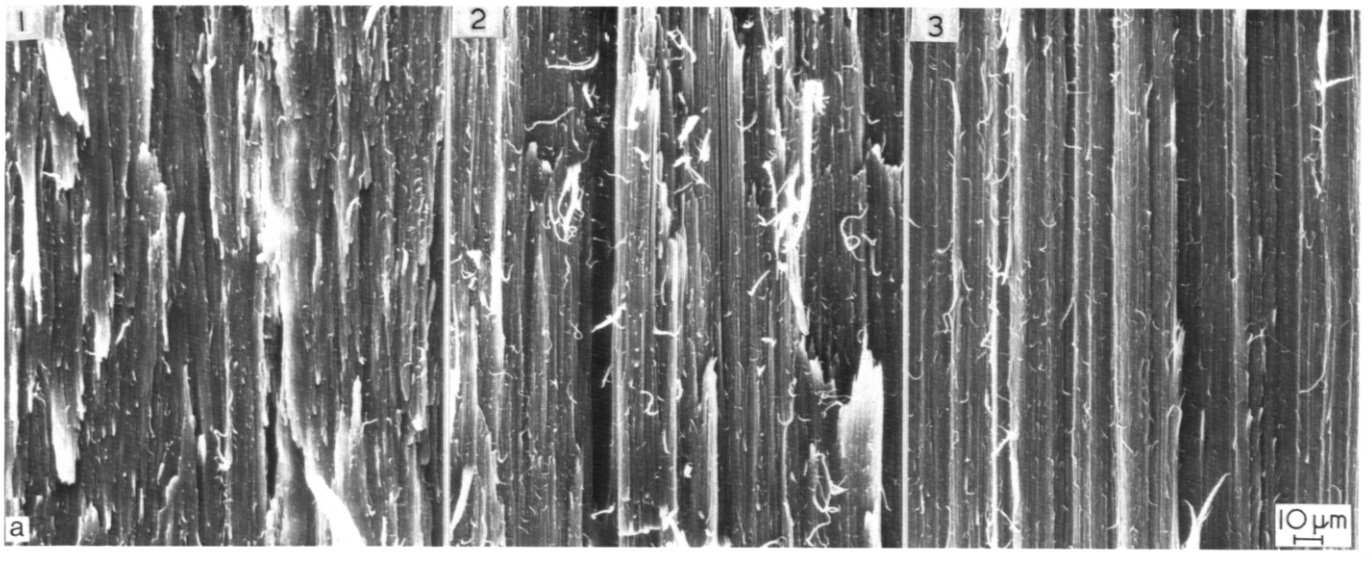

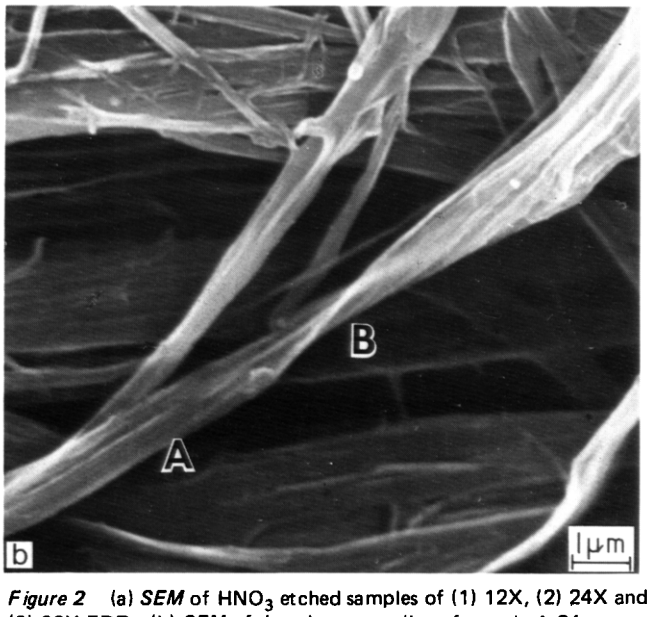

Figure 2 (a) *SEM* of HNO_3 etched samples of (1) 12X, (2) 24X and (3) 36X EDR. (b) *SEM* of detachment replica of sample A-24

Table 1 Properties of solid state extruded polyethylenes

Sample EDR	Tensile modulus (GPa)	Extrusion rate (mm min^{-1})	Weight % x_c	Density ρ
A-1	–	–	–	0.965
A-12	10	45	73	0.968
A-24	27	20	82	0.974
M-24	46	0.6	82	0.975
A-36	40	1.4	83	0.975

A = Alathon 7050 M_W = 59 000
M = Marlex 6003 M_W = 200 000

RESULTS AND DISCUSSION

For the Alathon series, the tensile modulus increases almost linearly with EDR from 10 GPa for A-12 to 40 GPa for A-36 as shown in *Table 1*. The 24 EDR Marlex sample had the highest observed modulus of 46 GPa.

Assuming that the crystalline regions in the fibre have the ideal crystal heat of fusion, the weight per cent degree of crystallinity χ_c increases with EDR from 73% for A-12 to 82% for A-24 and M-24, to 83% for A-36. All fibre melting curves were nearly identical with the peak position at $137 \pm 1°C$. Correspondingly, sample densities increase slightly with EDR (see *Table 1*).

Figure 2a shows *SEM* micrographs of the A-12 to A-36 EDR series. The HNO_3 treatment results in the preferential digestion and removal of the disordered portions of the sample which facilitates brittle longitudinal fracture and reveals the texture of the more or less crystalline remains. As the EDR increases, the fibre texture becomes smoother and better packed, fewer coarse fibrillar pieces are pulled out and the overall axial orientation appears higher. *Figure 2b* is a *SEM* of a detachment replica of sample A-24 but typical of all 4 extrudates. Fibrils form flat, ribbon-like structures, typically 1–2 μm in width with an aspect ratio of approximately 3:1 as determined from twisted regions (see regions A and B).

Detachment replicas also contain much smaller microfibrils than are shown in *Figure 2*. *Figure 3a* is a CTEM-BF image of sample A-12 with a number of 0.2–0.3 μm coarse fibrils and fine microfibrils as small as 250 Å in width. The lower contrast background is from the replica of the longitudinal fracture surface showing a highly aligned microfibre structure. The fibrils and microfibrils which adhered to the replica and were pulled out, are not as well aligned in the extrusion direction. The fibrils form an interconnected network (see regions indicated by arrows) quite similar to microfibril networks observed in cold drawn PE[41] and reflect the presence of interfibrillar tie molecules. *Figures 3b* and *c* show the A-24 and M-24 samples. The fibrils have become more highly aligned and uniform in diameter than the coarse fibrils in the A-12 sample. *Figure 3d* shows the *CTEM* BF image of the A-36 sample. The alignment and the nature of the structures is very similar to the A-24 and M-24 samples.

Electron diffraction patterns from the detached samples of the A-12, A-24, and A-36 specimens are shown in *Figures 4a–c*. All electron diffraction patterns were obtained from areas approximately 50 μm in diameter. The patterns show typical fibre symmetry. The layer lines become more discrete and the arcing of the 002 reflection decreases significantly for EDR greater than 12X. The pattern of the M-24 sample appears similar to that of the A-24 sample.

CTEM-DF images of the detached fibres were obtained using the combined 110 and 200 equatorial reflections. A

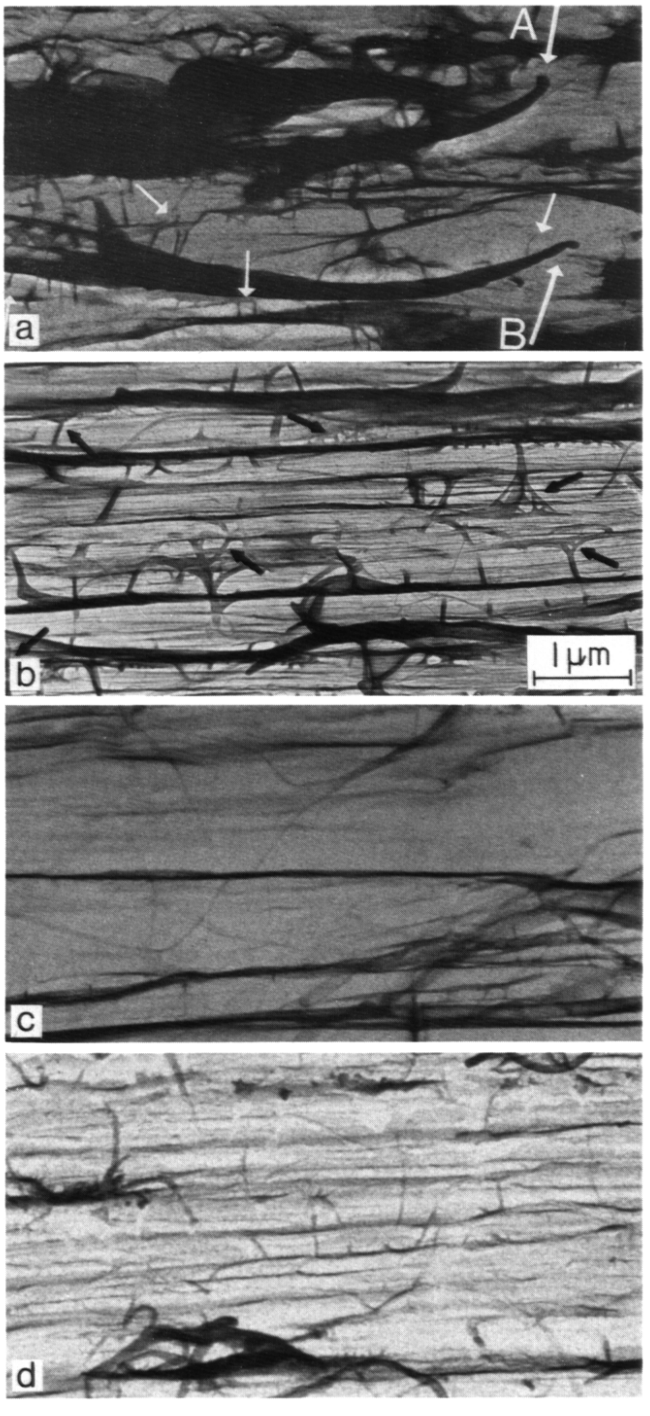

Figure 3 ***CTEM***-BF images of detachment replicas of samples (a) A-12, (b) A-24, (c) M-24, and (d) A-36. Arrows indicate junctions of the interconnected fibril network

typical image for the A-24 sample is shown in *Figure 5a*. Small diffracting crystallites the full width of the microfibres are randomly located along the fibrils. *Figure 5b* is a composite of several DF micrographs of the M-24 sample. These micrographs were chosen to illustrate two features of the morphology which are present in the M-24 sample and to a similar extent in the A-36 sample but absent in the A-12 and A-24 samples:

(1) a component of very long (1000–8000 Å) crystals (see white arrows)

(2) sequences of adjacent diffracting crystallites

The fraction of diffracting crystals per unit length of fibril expected for 'fibre symmetry' can be estimated as: [(number of independent nonmeridonal reflections used to form the DF image) × (average angular half width of the rocking curve for a crystallite of average diameter)]/360. For crystals of average diameter 250 Å, the angular half width is 1°, hence for combined 110–200 DF, less than 1% of the crystal population along the fibre should be in the diffraction condition for true fibre symmetry. DF images of A-12 and A-24 exhibit such a small population of randomly located diffracting crystallites. However, DF images of samples M-24 and A-36 (see *Figures 5b* and *7b*) show a substantial number of fibrils having sequences of 3–5 adjacent diffracting crystallites, each crystallite being separated by a 50–70 Å nondiffracting region. These results indicate while there is no lateral coherence between adjacent microfibrils [hence for a large enough area, the various fibril orientations will average to yield an electron diffraction pattern with apparent fibre symmetry] there is substantial axial coherence along a given microfibril (the extent of the 'crystallite colony') for the two highest modulus samples. Such coherence could be imparted by a thin (below the resolution of the DF image) central extended chain core crystal (shish or needle crystal) or as Ward[23,24] has suggested, by intercrystalline bridges (recall *Figure 1e*). With the present technique, it is not possible to distinguish between the two possibilities, since it is only the length of the invisibly thin connecting crystals which is different.

The crystal length distributions were studied quantitatively by measuring the lengths of the diffracting regions in the DF image and compiling crystal length histograms where the fraction of crystals of length , $n(l)$, is plotted *versus* l (see *Figure 6*). About 100 crystals were counted for each EDR sample. The number average l_N^{DF} and the weight average l_W^{DF} crystal lengths are indicated in *Figure 6* and in *Table 2*. The calculations overestimate the average crystal length since small crystals, less than about 50 Å are not counted since they are hard to distinguish from the background at the attainable resolution. The histograms show the crystal length distributions shifting to longer sizes with increasing EDR. Interestingly, samples A-12 and A-24 exhibit nearly the same crystal length distributions, although differing substantially in their mechanical properties. The distributions of the higher modulus M-24 and A-36 samples include crystals up to 900 Å in length (the rarer, up to 8000 Å long crystals are not included).

The crystallite size distribution determined by DF microscopy will also be influenced by any elastic and plastic distortion of the sample during sample preparation. Dark field will give a lower bound to crystal size since any distortions serve to reduce the coherently scattering region. The possible influence of elastic distortion on the observed crystallite size was explored using *STEM* n-beam annular DF[36]. This permits imaging of a greater number of crystals in a given area. In order to obtain serial DF images of a given area without image changes induced by radiation damage, optimum single image resolution was sacrificed (hence the *STEM* DF imageas appear somewhat more noisy than *CTEM* DF images). Pairs of *STEM* DF images were taken with the

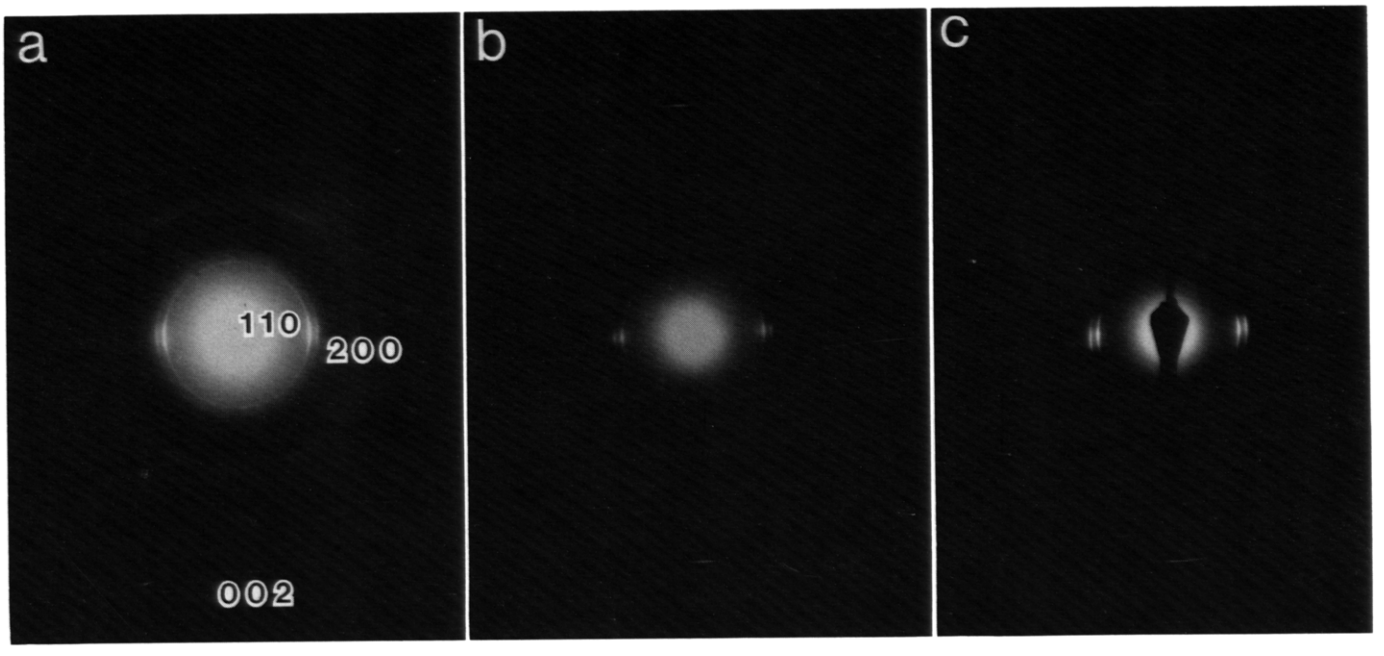

Figure 4 Electron diffraction patterns of detachment replicas of samples (a) A-12, (b) A-24, and (c) A-36

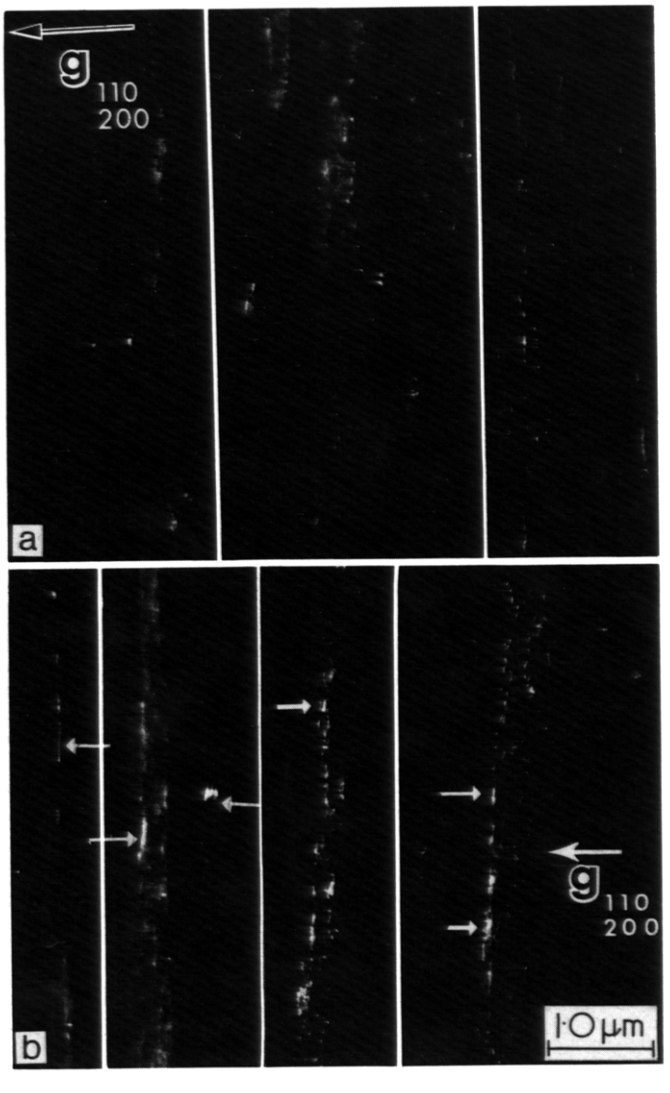

Figure 5 (a) *CTEM*-DF micrograph (g = 110 and 200) of sample A-24. (b) Composite of several *CTEM*-DF micrographs (g = 110 and 200) chosen to illustrate presence of long crystals (see arrowed regions) in sample M-24

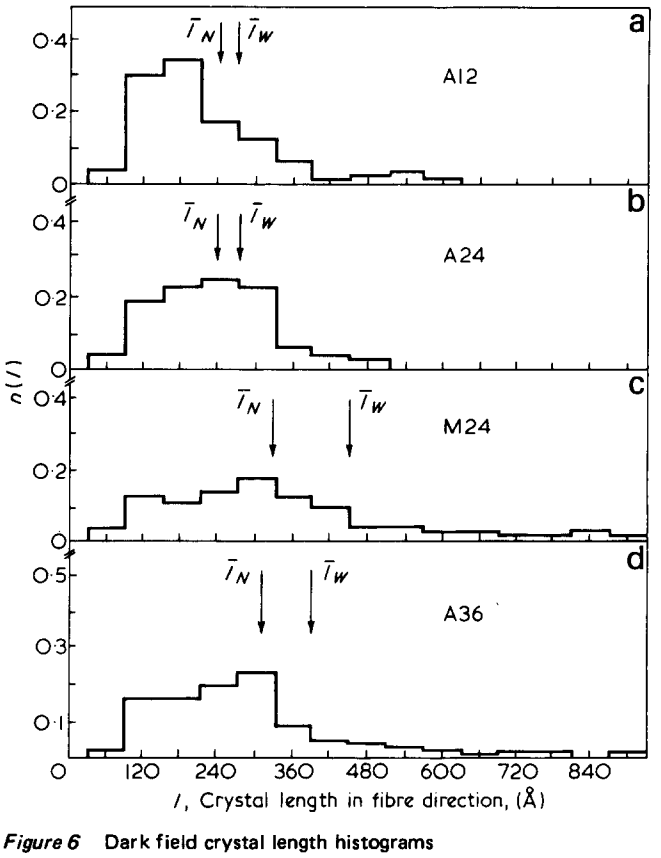

Figure 6 Dark field crystal length histograms

specimen tilted between exposures with respect to the incident beam direction (see *Figure 7a*). For accurate comparison of successive pictures of the same area, a transparent sheet was used where bright diffracting regions from one picture were marked (A). The transparent sheet could then be superposed on the tilted specimen micrograph (B) and in that way correspondence or noncorrespondence of about several dozen crystals per image was checked.

For a 1° tilt of the specimen between exposures, any long, continuous, but elastically bent crystalline regions

should become diffracting in regions just adjacent to those previously diffracting. The observed effect of a small tilt is to leave many diffracting regions unchanged (hence eliminating the need to consider changes induced by radiation damage) while a few diffracting crystallites disappear and a few new diffracting crystallites appear at random locations. A complete series of micrographs over various angles of tilt is required to completely assess elastic bending, as well as to explore for the possible presence of large angle tilt (twin or kink) boundaries. Because of radiation damage, such detailed studies are not possible. Pairs of DF images have been obtained for large ($\sim 35°$) tilts as shown in *Figure 7b*. Experiments of this type are problematic because of focus changes and the difficulty of correct image registration for comparison purposes. For the few good micrograph pairs we were able to obtain, we could find no systematic image changes suggestive of twins or kink boundaries. However, further evidence of 'crystallite colonies' is noted (see arrowed regions in *Figures 7b*).

Plastic distortion of long crystals due to sample preparation does not appear significant since:

(1) Thin fibres dispersed by nitric acid etching exhibited approximately the same DF crystallite sizes as detachment replica fibres.

(2) Some long crystals have been found in the A-36 and M-24 samples. Their absence in the A-12 and A-24 samples suggests a real effect.

In summary, the solid state extruded high density polyethylene samples are microfibrillar. The microfibril bundles are ribbon-like with a cross-sectional aspect ratio of $\sim 3{:}1$. This ribbon texture extends down to the primary 120–250 Å wide microfibrils. The DF investigations show an increase in average crystallite size along the fibre direction with increasing EDR. The A-12 and A-24 samples appear similar to conventionally drawn fibres, i.e. crystalline regions alternating with intervening noncrystalline regions along the microfibrils. The microstructures of the higher molecular weight sample M-24 and the highest extrusion draw ratio sample A-36 however contain a broader crystallite size distribution and perhaps more significantly, a component of long (1000–8000 Å) crystals as well as thin crystalline bridges (or needle crystals) which impart coherence to sequences of adjacent crystallites along the fibre and likely account for the high tensile modulus observed for these two extrudates.

Table 2 Axial crystallite size determined by dark field microscopy

Sample EDR	DF $l_{c,N}$ (Å)	DF $l_{c,w}$ (Å)
A-12	240	270
A-24	240	270
M-24	340	475
A-36	310	390

ACKNOWLEDGEMENT

The authors thank Dr M. Watts and Mr M. Daniels for sample preparation and for mechanical testing. The *SEM* micrographs of the HNO_3 treated extrudates were kindly furnished by Dr K. Shimamura. The authors would also like to thank Professor R. S. Stein for fruitful discussions. Financial support (for E.S.S.) was from the NSF through grant DMR 77-24955 (E.L.T.) and the Materials Research Laboratory of the University of Massachusetts. The support for sample preparation by NSF Engineering through grant DMR 79-25564 (R.S.P.) is gratefully acknowledged.

REFERENCES

1 Peterlin, A. *Polym. Eng. Sci.* 1974, **14**, 627
2 Peterlin, A. *Polym. Eng. Sci.* 1979, **19**, 118
3 Capiati, N., Kojima, S., Perkins, W. and Porter, R. S. *J. Mater. Sci.* 1977, **12**, 334
4 Taylor, Jr., W. N. and Clark, E. S. *Polym. Eng. Sci.* 1978, **18**, 518
5 Pennings, A. J., Schouteten, C. J. H. and Kiel, H. M. *J. Polym. Sci.* 1972, **C38**, 167
6 Wobser, G. and Blasenbrey, S. *Kolloid Z.-Z. Polym.* 1970, **241**, 985
7 Barham, P. J. and Keller, A. *J. Polym. Sci., Polym. Lett. Edn.* 1979, **17**, 591
8 Capaccio, G. and Ward, I. M. *Polym. Eng. Sci.* 1975, **15**, 219

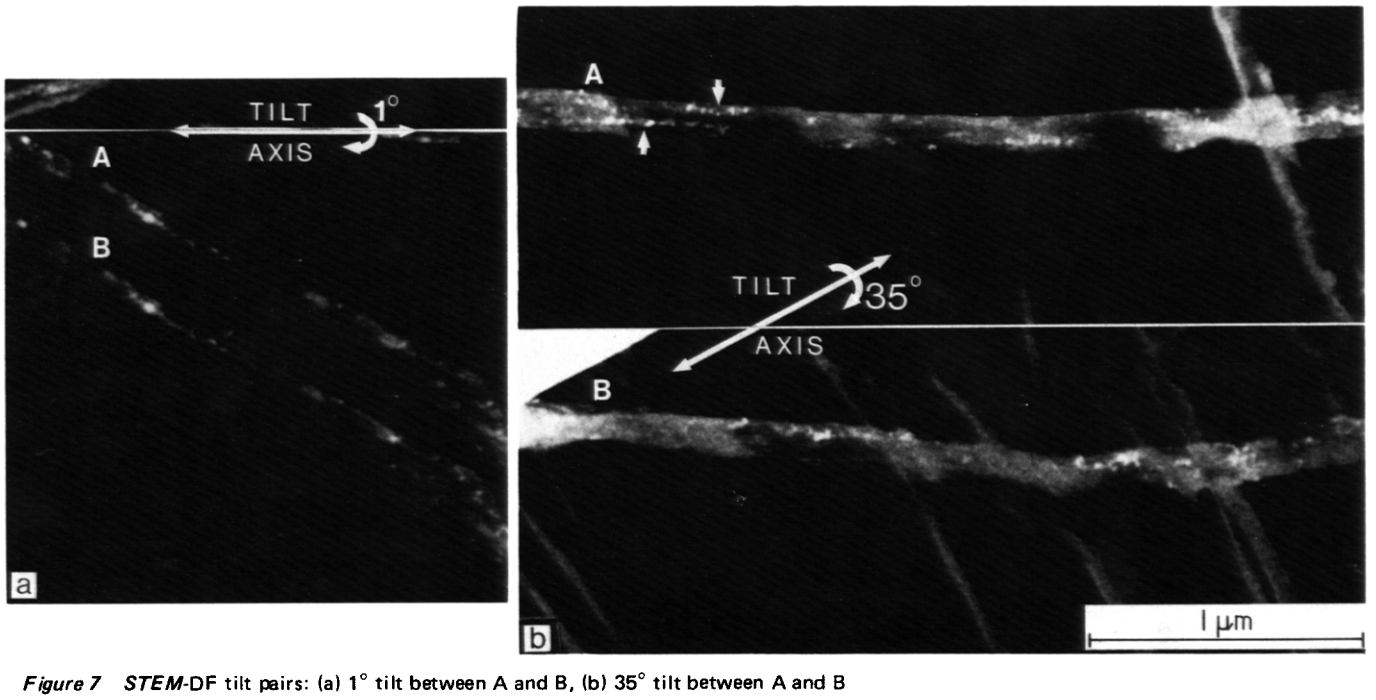

Figure 7 *STEM*-DF tilt pairs: (a) 1° tilt between A and B, (b) 35° tilt between A and B

9 Barham, P. J. and Keller, A. *J. Mater. Sci.* 1976, **11**, 27
10 Wu, W., Simpson, P. G. and Black, W. B. *J. Polym. Sci., Polym. Phys. Edn.* 1980, **18**, 751
11 Imada, K., Yamamoto, T., Shigematsu, K. and Takayangi, M. *J. Mater. Sci.* 1971, **6**, 537
12 Zachariades, A. E., Griswold, P. D. and Porter, R. S. *Polym. Eng. Sci.* 1979, **19**, 441
13 Adams, W. W., Sherman, E. S., Briber, R. M., Porter, R. S., Thomas, E. L. and Lin, J. S. *Polymer* in press
14 Meyer, K. H. and Mark, H. 'Der Aufbau der Hochpolymeren Naturstoffe', Leipzig, 1930
15 Staudinger, H. 'Die Hochmolekularen Organischen Verbindungen', Springer, Berlin, 1932
16 Hess, K. and Kiessig, H. *Naturwissenschaften* 1943, **31**, 171
17 Peterlin, A. *J. Polym. Sci.* 1965, **C9**, 61
18 Peterlin, A. *Polym. Eng. Sci.* 1978, **18**, 488
19 Prevorsek, D. C., Harget, P. J., Sharma, R. K. and Reimscheussel, A. C. *J. Macromol. Sci., Phys.* 1973, **B-8**, 127
20 Fischer, E. W. and Goddar, H. *J. Polym. Sci.* 1969, **C16**, 4405
21 Porter, R. S. *Polym. Prepr., Am. Chem. Soc.* 1971, **12**, No. 2
22 Clark, E. S. and Scott, L. S. *Polym. Eng. Sci.* 1974, **14**, 682
23 Clements, J., Jakeways, R. and Ward, I. M. *Polymer* 1978, **19**, 639
24 Gibson, A. G., Davies, G. R. and Ward, I. M. *Polymer* 1978, **19**, 683
25 Frye, C. J., Ward, I. M., Dobb, M. G. and Johnson, D. J. *Polymer* 1979, **20**, 1201
26 Grubb, D. T. and Keller, A. *Colloid Polym. Sci.* 1978, **256**, 218
27 Bourret, A., Chanzy, H. and Lazaro, R. *Biopolymers* 1972, **11**, 893
28 Petermann, J., Miles, M. and Gleiter, H. *J. Polym. Sci., Polym. Phys. Edn.* 1979, **17**, 55
29 Weeks, N. E., Mori, S. and Porter, R. S. *J. Polym. Sci., Polym. Phys. Edn.* 1975, **13**, 2031
30 Capiati, N. J. and Porter, R. S. *J. Polym. Sci., Polym Phys. Edn.* 1977, **15**, 1427
31 Mead, W. T. and Porter, R. S. *J. Appl. Phys.* 1976, **47**, 4278
32 Zachariades, A. E., Mead, W. T. and Porter, R. S. in Ultrahigh Modulus Polymers, (Eds. A. Ciferri, and I. M. Ward), Applied Science Publishers, London, UK, 1978
32 Zachariades, A. E., Mead, W. T. and Porter, R. S. in 'Ultrahigh Modulus Polymers', (Eds. A. Ciferri and I. M. Ward), Applied
34 Geil, P. in 'Polymer Single Crystals', Wiley Interscience, New York, 1963
35 Palmer, R. P. and Cobbold, A. J. *Makromol Chem.* 1964, **74**, 174
36 Sherman, E. S., Adams, W. W. and Thomas, E. L. *J. Mater. Sci.* 1981, **16**, 1
37 Grubb, D. T. *J. Mater. Sci.* 1974, **9**, 1715
38 Thomas, E. L., Sass, S. L. and Kramer, E. J. *Philos. Mag.* 1974, **30**, 335
39 Shimamura, K., Murakami, S., Tsuji, M. and Katayama, K. *Trans. Soc. Rheol. Jpn.* 1979, **7**, 42
40 Ke, B. *J. Polym. Sci.* 1960, **42**, 15
41 Tarin, P. T. and Thomas, E. L. *Polym. Eng. Sci.* 1979, **19**, 1017